Geophysical Research Letters®

Key Points:

- During a storm-time substorm, 2 MeV electron precipitation was associated with the auroral bulge
- The magnetospheric source region of the auroral bulge and the radiation belt (RB) overlapped during this substorm
- We deduce that the source region of the auroral bulge and RB electrons was in the newly dipolarized magnetosphere

On the Spatial Relationship Between the Aurora and Relativistic Electron Precipitation During a Storm-Time Substorm

M. Shumko[1], A. Artemyev[2], S. Raptis[1], Y. Zou[1], D. L. Turner[1], A. Y. Ukhorskiy[1], C. Gabrielse[3], G. K. Stephens[1], I. J. Cohen[1], C. Wilkins[2], E. Tsai[2], S. Ohtani[1], B. Gallardo-Lacourt[4], K. Sorathia[1], V. Sergeev[5], J. W. Gjerloev[1], E. Donovan[6], E. Spanswick[6], V. Angelopoulos[2], and A. N. Jaynes[7]

[1]The Johns Hopkins University Applied Physics Laboratory, Laurel, MD, USA, [2]Department of Earth, Planetary, and Space Sciences, University of California Los Angeles, Los Angeles, CA, USA, [3]The Aerospace Corporation, El Segundo, CA, USA, [4]NASA Goddard Space Flight Center, Greenbelt, MD, USA, [5]Department of Geophysics, Physical Faculty, University of St. Petersburg, Petersburg, Russia, [6]Department of Physics and Astronomy, University of Calgary, Calgary, AB, Canada, [7]Department of Physics & Astronomy, University of Iowa, Iowa City, IA, USA

Abstract During substorms, Earth's magnetotail undergoes rapid dipolarization, driving Earthward plasma flows that decelerate and dissipate energy upon encountering the dipole magnetic field in the nightside transition region. This region mediates the interaction between the magnetotail, inner magnetosphere, and the ionospheric auroral zone, though significant mapping uncertainties obscure the precise link and particle acceleration processes. Using data from THEMIS, TREx, and ELFIN, we analyze a storm-time substorm on 4 September 2022, establishing a relationship, that is, not a causation, between magnetospheric and ionospheric dynamics. Following a dipolarization, the auroral bulge overlapped with the footprints of the electron isotropy boundary (IB) and the outer radiation belt. Notably, the precipitating electron energies reached at least 2 MeV in the bulge, exceeding previous reports. By comparing the latitudes of the electron IB with respect to the auroral bulge, we deduce that the sources of both auroral and relativistic precipitation were confined in the dipolarized region.

Plain Language Summary Explosive magnetospheric substorms and beautiful auroral displays are signatures of rapid reconfiguration of Earth's magnetic field from a stretched to a more dipolar configuration. The global reconfiguration is known as dipolarization, a phenomenon that occurs simultaneously with bright auroral displays. The dipolarization, aurora, and the hazardous radiation belt (RB) electrons are likely linked, though significant magnetic mapping uncertainties obscure the precise link and the particle acceleration processes involved. Here, we study this system with a fortuitous combination of satellites and ground-based auroral imagers. After a dipolarization, the aurora overlapped with the energetic electrons prescribed to the outer RB. These findings reveal that during the peak of a substorm, the bright part of the auroral oval is sometimes contained within the newly reconfigured magnetic field, highlighting the intricate relationship between cislunar space and Earth's atmosphere.

1. Introduction

Substorms are explosive releases of energy routinely occurring in Earth's magnetotail and its embedded current sheet (e.g., Birn et al., 2012; Sergeev, Angelopoulos, & Nakamura, 2012; Sitnov et al., 2019, and references within). They are typically characterized by a reconfiguration of magnetotail field lines from a stretched to a more dipolar geometry (Akasofu, 1964; Kamide & Chian, 2007; McPherron et al., 1973). This dipolarization process accelerates and transports plasma sheet (PS) particles Earthward via fast flows and dipolarizing flux bundles (e.g., Birn et al., 2011; Birn et al., 2012; Gabrielse et al., 2014, 2016, 2017; Runov et al., 2011) toward the nightside transition region (NTR; Donovan, 2016; Gabrielse et al., 2023, and references within). The NTR is the interface between Earth's stretched and dipolar field lines, and is where fast flows tend to rapidly break, deflect, and dissipate their energy (Sergeev, Nishimura, et al., 2012; Shiokawa et al., 1997).

The NTR is highly dynamic during substorms. PS particles are periodically injected through it and outer radiation belt (RB) electrons are energized to relativistic (>500 keV) energies (e.g., D. Turner et al., 2015; Gabrielse et al., 2017). Furthermore, during the substorm expansion phase, the NTR and the dipolarized region expand

Software: M. Shumko, B. Gallardo-Lacourt, V. Angelopoulos
Supervision: D. L. Turner, A. Y. Ukhorskiy, I. J. Cohen
Validation: S. Raptis
Visualization: M. Shumko
Writing – original draft: M. Shumko, A. Artemyev
Writing – review & editing: M. Shumko, A. Artemyev, S. Raptis, Y. Zou, D. L. Turner, C. Gabrielse, G. K. Stephens, I. J. Cohen, C. Wilkins, E. Tsai, S. Ohtani, K. Sorathia, V. Sergeev, J. W. Gjerloev, E. Spanswick, A. N. Jaynes

azimuthally and radially outward, driving the formation of large-scale and meso-scale field-aligned currents (FACs), and scattering electrons into the high-latitude ionosphere (e.g., D. Baker et al., 1981; Lopez et al., 1990; Reeves et al., 1996; Spanswick et al., 2005, 2010; Dubyagin et al., 2011; Gabrielse et al., 2023). There, precipitating 1–10 s keV electrons associated with FACs produce discrete auroral arcs, while 10 s keV electrons generate diffuse aurora (Paschmann et al., 2003; Nishimura et al., 2020, and references within). The radial and azimuthal expansion of the dipolarized region corresponds to a poleward and westward expansion of the aurora, with a multitude of diffuse and discrete auroral forms which occur inside a larger region termed the auroral bulge (Nishimura, Lyons, et al., 2010; L. R. Lyons et al., 2018; Paschmann et al., 2003; Henderson, 2009; Ohtani et al., 2021).

While the aforementioned phenomena have largely been studied in their magnetospheric or ionospheric contexts, connecting the two regions is crucial to understand magnetosphere-ionosphere coupling. Prior studies found that the aurora associated with substorms is driven by sources on closed magnetic field lines in the vicinity of the NTR and the inner PS (Donovan, 2016; Baker et al., 1996; Samson et al., 1992; D. N. Sergeev, Angelopoulos, & Nakamura, 2012; Sergeev, Nishimura, et al., 2012). However, large magnetic field mapping uncertainties often preclude the association of ionospheric precipitation to its magnetospheric source (Nishimura, Bortnik, et al., 2010; Shevchenko et al., 2010). Nevertheless, we can use the change in the magnetic topology and particle scattering characteristics across the NTR to identify the sources of precipitation originating from the inner magnetosphere or the magnetotail (Paschmann et al., 2003).

In the stretched magnetotail, the magnetic field radius of curvature is smaller, or is on the order of, the electron gyroradius ($R_C < \rho_e$). Specifically, where $R_C/\rho_e < 8$, the first adiabatic invariant is violated, causing particles to move chaotically and be isotopically scattered and lost in the ionosphere via magnetic field line curvature scattering (FLCS) (Lyons & Speiser, 1982; Sergeev et al., 1983). In the NTR, R_C/ρ_e rapidly increases in the Earthward direction as the field becomes more dipolar until $R_C/\rho_e > 8$ and electrons become trapped (e.g., Ripoll et al., 2020; Sergeev et al., 1983; Wilkins et al., 2023).

At ionospheric altitudes, the separation between the trapped and precipitating particles scattered via FLCS is called the isotropy boundary (IB). The IB is both energy- and species-dependent, since gyroradii depends on both (Sergeev et al., 1983). The IB is readily observed in low Earth orbit (LEO), where particle populations (PS vs. RB) can be differentiated with energy-resolved omnidirectional fluxes (j), as well as with the fluxes inside ($j_\parallel$), and just outside ($j_\perp$), the bounce loss cone. In LEO, the IB appears as an energy-dependent transition between electrons with $j_\parallel/j_\perp \sim 1$ (i.e., isotropic) on the poleward side, and $j_\parallel/j_\perp < 1$ (i.e., anisotropic) on the equatorward side (Sergeev et al., 1983). During quiet conditions the IB typically has an energy-latitude pattern with lower energy electrons isotropically scattering at higher latitudes (Newell et al., 1996; Wilkins et al., 2023, 2024). Contrary to the proton IB that is often observed at all local times and has been investigated statistically (e.g., Sergeev et al., 1983; Sergeev et al., 1997; Shi et al., 2024; Yue et al., 2014), the electron IB has been investigated much less (see discussion in Imhof et al., 1979; Sergeev, Nishimura, et al., 2012; Gabrielse et al., 2022; Wilkins et al., 2023). This is partially due to the electron IB being occasionally obscured by wave-particle scattering on the Earthward side, driven by waves such as electromagnetic ion cyclotron and chorus (A. V. Artemyev et al., 2024).

Guided by 10s–100 keV X-ray balloon measurements, Barcus (1965) and Lazutin and Rosenberg (1986), assumed that the expansion phase aurora maps to the outer RB—Earthward of the NTR. This assumption was further bolstered by recent studies associating energetic RB precipitation (>30 keV up to 100 s keV) with substorm activity (Gabrielse et al., 2019; Sergeev et al., 2019; Troyer et al., 2022). However, to our knowledge a direct confirmation of this assumption has yet to be made with aurora and electron precipitation observations. We provide the most compelling evidence of this assumption here.

We present a fortuitous triple conjunction on 4 September 2022 between the Time History of Events and Macroscale Interactions during Substorms (THEMIS; Angelopoulos, 2009) mission, the Transition Region Explorer (TREx; Spanswick & Donovan, 2023) auroral all-sky imagers (ASIs), and the Electron Losses and Fields Investigation (ELFIN; Angelopoulos et al., 2019). This conjunction revealed a complete spatial overlap of the auroral bulge and <2 MeV electron precipitation during a well-timed dipolarization and poleward expansion during a moderate storm. By comparing the latitudes of the electron IB with respect to the auroral bulge, we deduce that the sources of both auroral and relativistic precipitation were confined to the dipolarized region.

2. Instruments and Methodology

The THEMIS mission consists of three identical satellites launched on 17 February 2007 into highly elliptical orbits with a 31-hr orbital period (Angelopoulos, 2009). Each probe spins with a 3-s period and contains five instruments that measure ions and electrons from ~5 eV to ~1 MeV and electromagnetic fields and waves from DC to >4 kHz (Angelopoulos et al., 2008; Auster et al., 2008; Bonnell et al., 2009; McFadden et al., 2008; Roux et al., 2008).

The twin 3U ELFIN CubeSats were launched on 15 September 2018 and ELFIN-A, which we primarily use here, de-orbited shortly after this event on 17 September 2022 (Tsai et al., 2024). During the conjunction, ELFIN was in a polar LEO at ~270 km altitude and a 90-min orbit period (Angelopoulos et al., 2020, 2023). Each CubeSat was equipped with an energetic particle detector that measured 50 keV to 7 MeV electrons in 16 logarithmically-spaced energy channels. ELFIN spun with a nominal 2.7-s period, during which they observed fluxes in the bounce and drift loss cones. As we describe in the Text S1 in Supporting Information S1, we binned the spin-resolved ELFIN-EPD fluxes in time, energy, and pitch angle, and calculated j, $j_\parallel$, and $j_\perp$. With ELFIN we can identify a multitude of particle populations and scattering mechanisms via their j spectrum and energy-dependent $j_\parallel/j_\perp$ ratio (A. V. Artemyev et al., 2021; A. Artemyev et al., 2022; Angelopoulos et al., 2023; Wilkins et al., 2023; Tsai et al., 2024; Zhang, Artemyev, et al., 2022). A ratio $j_\parallel/j_\perp \ll 1$ indicates an empty loss cone with only drifting electrons, while a ratio $j_\parallel/j_\perp \sim 1$ indicates that the loss cone is full of precipitating electrons.

The TREx-RGB array consists of "true color" ASIs deployed across Canada with overlapping fields of view—providing regional-scale observations of the aurora (Gillies et al., 2020). The auroral light first passes through a fisheye lens that expands each imager's field of view to nearly 180°, and at the end is recorded by a highly-sensitive Canon CMOS sensor. Here we use the 480 × 553 pixel, 3-s cadence images (Liang et al., 2023). To clearly identify auroral features before and after the substorm we normalized the images using contrast stretching. To compare the aurora with satellite measurements, we use skymap calibration files, derived by the instrument team, to map the auroral images from pixel coordinates to geographic coordinates, assuming a 110 km emission altitude. For each time stamp, we merged the mapped images from each ASI into a mosaic. In the overlapping region between neighboring ASIs, we only kept the highest elevation pixels.

For this case study, the THEMIS probes are in the PS and thus provide the magnetospheric perspective. On substorm time scales, THEMIS is effectively stationary and is probing the temporal evolution of the near-Earth magnetotail. Similarly, the TREx ASIs are stationary on these time scales and thus observe the time evolution of auroral precipitation over a large area. In contrast to this, ELFIN rapidly—within five minutes—crossed the high-latitude ionosphere, and observed precipitation originating from sources corresponding to L-shells ranging from the inner magnetosphere to the distant magnetotail.

3. Results

Figures 1a–1d shows the solar wind conditions and geomagnetic indices around the 4 September 2022 substorm (Gjerloev, 2012; King & Papitashvili, 2005). Figure 1a shows the z-component of the interplanetary magnetic field (B_z) which was predominately negative in the hours preceding the substorm. Figure 1b shows the solar wind speed increasing from 500 to 680 km/s. The fast solar wind, together with the negative B_z, effectively coupled to the magnetosphere. Figures 1c and 1d show the SuperMag lower electroject (SML; Newell & Gjerloev, 2011) and the SuperMag ring current (SMR; Newell & Gjerloev, 2012) indices which show multiple substorms during the main phase of the storm. Specifically, the vertical dashed black line corresponds to the substorm which is the focus of this study. The substorm onset occurred at 04:12 UT (Newell & Gjerloev, 2011), during the main phase of a storm (SMR = −25 nT at 4 UT, and SMR_{min} = −70 nT at 12 UT). During the substorm expansion phase, the SuperMag lower index dipped to −880 nT. Lastly, panel (e) summarizes the auroral activity during this time period with a keogram, constructed from the TREx-RGB Gillam and Pinawa ASIs along THEMIS-A's longitude, with Pinawa's keogram superposed above Gillam's. The resulting keogram is a function of time and λ, the altitude adjusted corrected geomagnetic magnetic latitude (Shepherd, 2014). The keogram shows multiple poleward expansions of the aurora between 4 and 7 UT.

The conjunction occurred in the pre-midnight sector, with Figures 1f and 1g showing the equatorial locations of the THEMIS probes on field lines traced with the T89 magnetic field model (Tsyganenko, 1989). Of the three probes, T89 maps THEMIS-A nearest to the neutral sheet, which is confirmed by the relatively small $|B_x|$
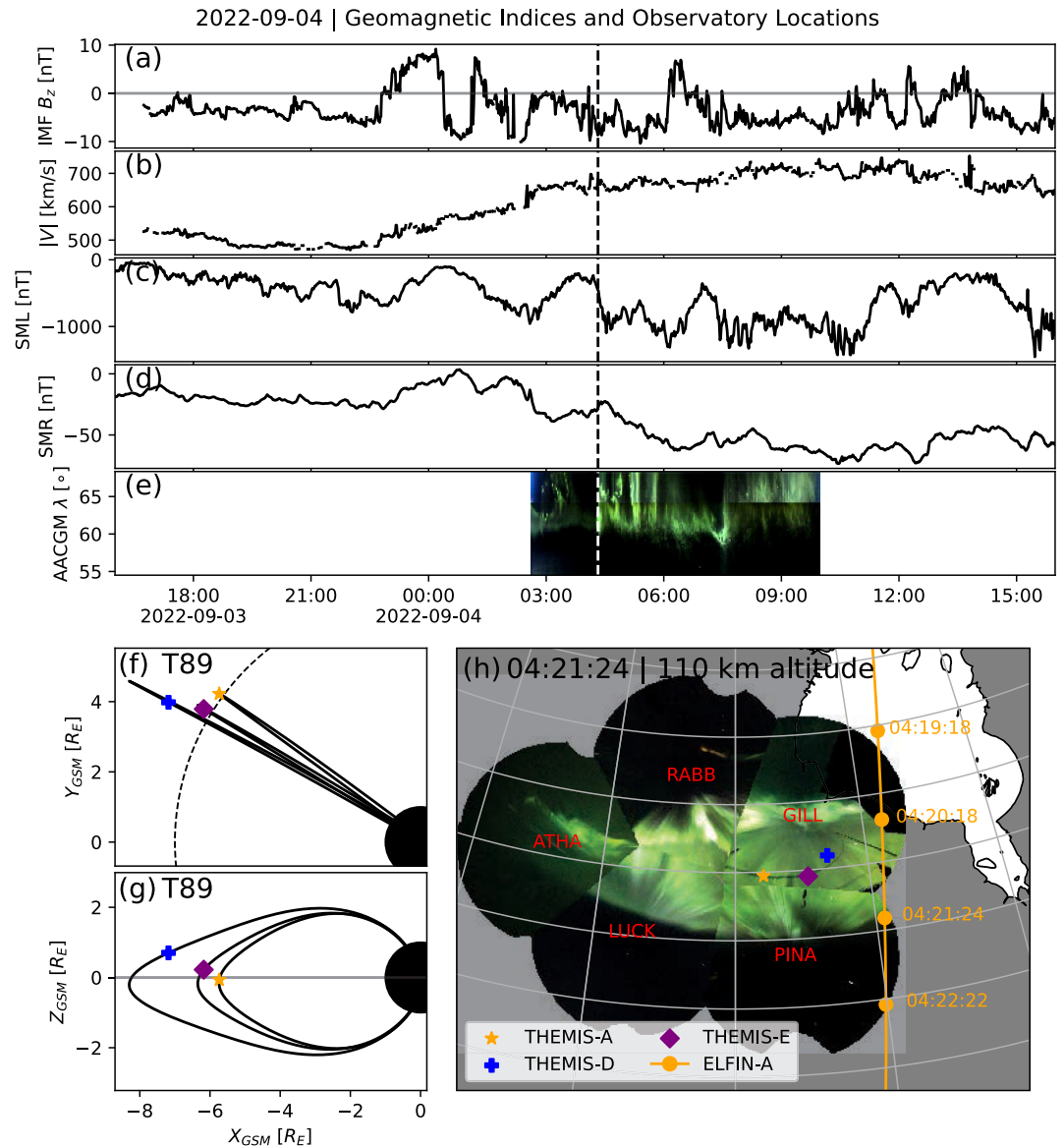
Figure 1. Observatory locations, geomagnetic conditions, and solar wind conditions for the substorm event. Panels (a) and (b) show the solar wind B_z and speed. Panels (c) and (d) show the SuperMag lower electrojet (SML) and SuperMag ring current (SMR) indices. Panel (e) shows a TREx-RGB keogram assembled from the Gillam and Pinawa all-sky imagers (ASIs). The vertical dashed line spanning panels (a–e) is at the time of the substorm studied here. Panels (f) and (g) show the x-y and x–z projections of the THEMIS probe locations, with their field lines traced using the T89 magnetic field model. For reference, the dashed curve in panel (f) is a segment of an $R = 7$ R_E circle. Panel (h) shows the 110 km footprints of THEMIS and ELFIN-A above a TREx mosaic assembled from the five ASIs at 04:21:24. The orange line shows the ELFIN-A footprints, with four locations annotated with circles and time stamps along the footprint.

component of the magnetic field shown in Figure 2a. Lastly, Figure 1h shows the 110-km altitude ionospheric footprints of THEMIS, ELFIN, and a representative TREx mosaic. We annotate ELFIN-A footprints at four times to highlight how rapidly it crossed the auroral region.

Figure 2 shows the magnetotail conditions during this substorm. Figure 2a shows that THEMIS-A was located near the central PS ($B_x \sim 0$). Right before the dipolarization (~4:17 UT), the magnetic inclination ($B_z / \sqrt{B_x^2 + B_y^2}$) in Figure 2b was 0.51 which indicates that THEMIS-A was near the central PS and the near-Earth magnetic field lines were stretched at $R = 7$ R_E (Raptis et al., 2024). Then after the dipolarization (~4:21 UT) the magnetic inclination increased to 0.98 and the magnetic field became highly dipolar. During this
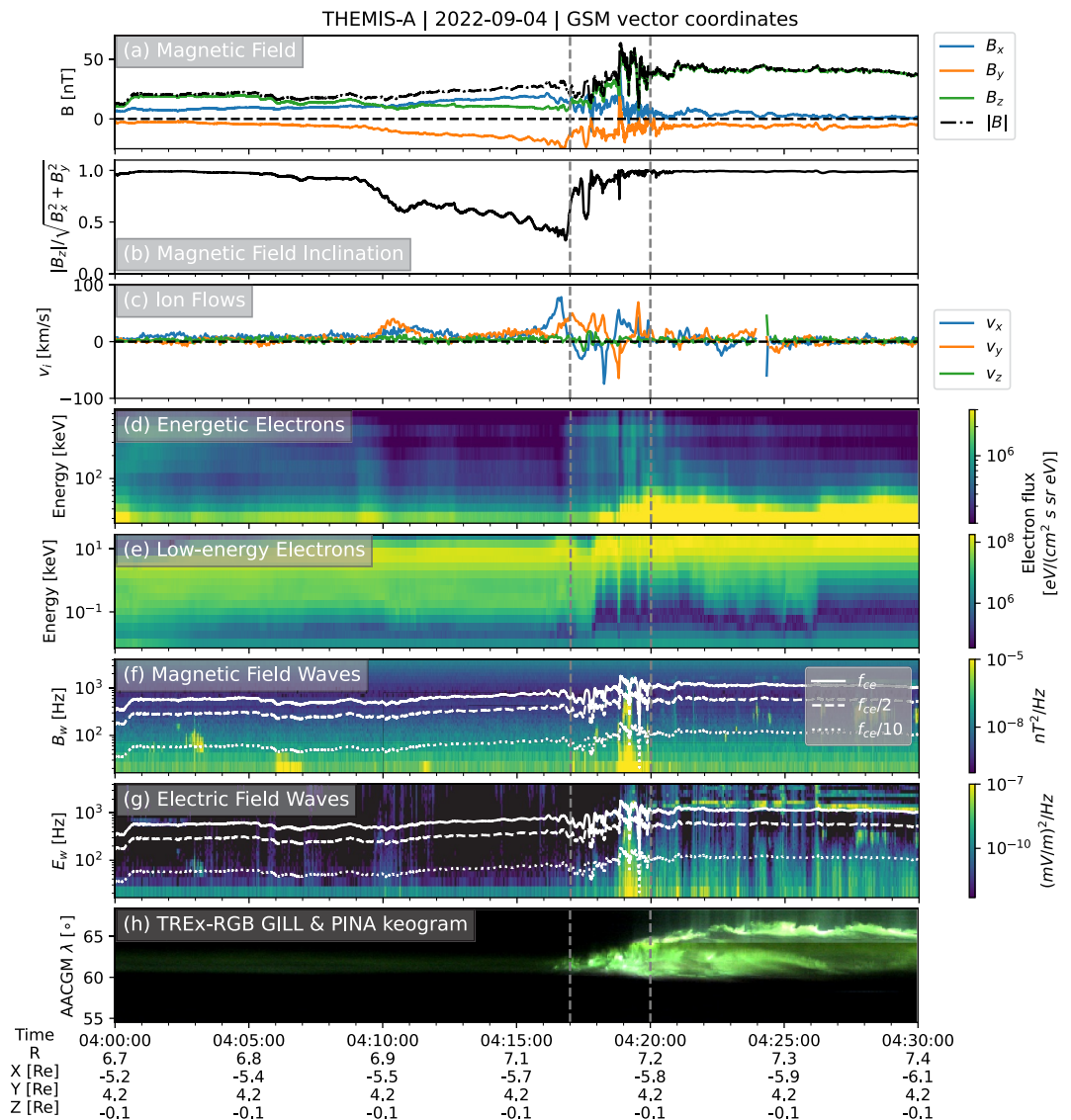
Figure 2. THEMIS-A and TREx all-sky imager (ASI) observations of the substorm. Panels (a–g) show THEMIS-A data, while Panel (h) shows the TREx data. Panel (a) shows the magnetic field, panel (b) shows the magnetic field inclination, panel (c) shows the ion flows, panels (d) and (e) show the energetic and low-energy electrons, panels (f) and (g) show the magnetic and electric wave power, as well as lines at f_{ce}, $0.5f_{ce}$, and $0.1f_{ce}$ frequencies. Lastly, panel (h) shows the keogram assembled with images taken by Gillam and Pinawa TREx-RGB ASIs. See Movie S1 for an animated TREx mosaic. All vectors are in geocentric solar magnetospheric coordinate system and the two vertical dashed gray lines correspond to the approximate start and end time of the dipolarization.

four-minute dipolarization, THEMIS-A observed typical substorm signatures including fast ion flows and accelerated low- and high-energy electrons. Furthermore, it observed electric and magnetic field waves with frequencies below a tenth of the electron gyrofrequency ($f < 0.1f_{ce}$), as well as structured wave emissions in the lower-band chorus frequency range ($0.1f_{ce} < f < 0.5f_{ce}$) which can scatter 10 s keV-MeV electrons (e.g., Chen et al., 2020; Miyoshi et al., 2020). At this time Figure 1f shows that both THEMIS-D and -E were magnetically connected further tailward, providing limited additional context to our analysis. Nonetheless, for completeness we show their observations in Figures S1 and S2 in Supporting Information S1.

The aurora associated with this dipolarization was observed by TREx. Figure 2h summarizes the auroral activity during the substorm with a keogram in the same format as Figure 1e. The keogram shows the sudden brightening of a faint arc at 4:17 UT, followed by the poleward expansion of the aurora. As the substorm progressed, the
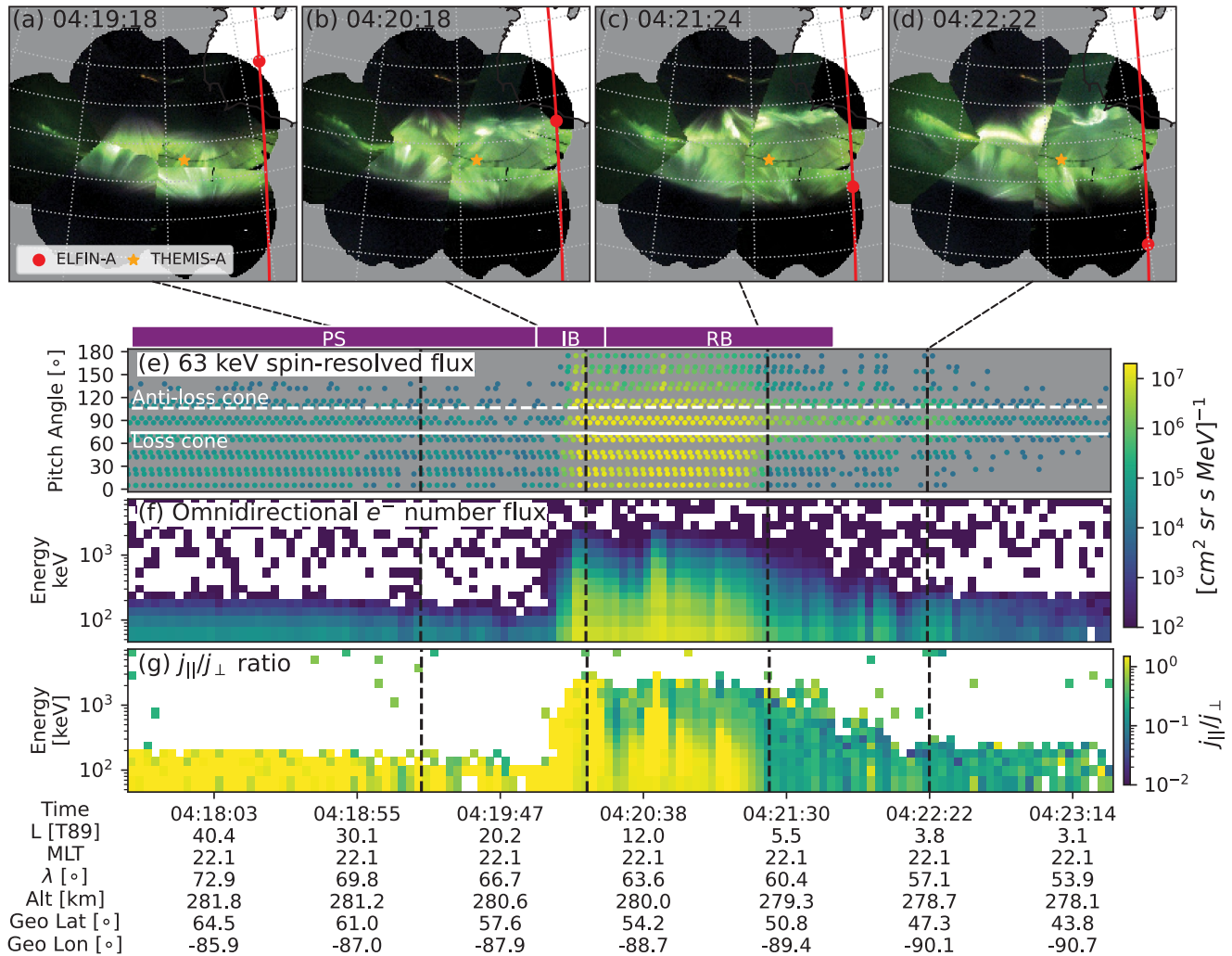
Figure 3. Ground and low Earth orbit observations of the substorm made by TREx all-sky imagers and ELFIN-A. Panels (a–d) show a montage of TREx mosaics, mapped to 110 km, for times annotated in the upper-left corner. The red solid line is the entire ELFIN-A trajectory mapped to 110 km, and the red dot is the instantaneous ELFIN-A location at each time. Panel (e) shows the spin-resolved 63 keV electron fluxes as a function of pitch angle and time. The solid and dashed white lines and the loss and anti-loss cone angles, respectively. Panel (f) shows the omnidirectional > 50 keV electron number fluxes observed by ELFIN-A. Lastly, panel (g) shows the $j_\parallel/j_\perp$ ratio as a function of energy and time. Above panel (e), we annotate the plasma sheet, isotropy boundary and outer radiation belt regions. See Movie S2 for an animated version of this figure.

aurora consisted of a bright wavy arc at the poleward-edge, and diffuse-like aurora with some internal structure which we refer to as structured diffuse aurora (SDA; Nishimura et al., 2020) equatorward of it. This can be more clearly seen in the TREx mosaic in Movie S1 which shows diffuse auroral light, structured wavy arcs, and other dynamic auroral features.

Figure 3, together with Movie S2, show the spatial and temporal evolution of the aurora and the relativistic precipitation observed by TREx and ELFIN-A, respectively. During the auroral poleward expansion phase, ELFIN-A passed through the eastern edge of the TREx field of view, and observed electron precipitation up to 2 MeV. Figures 3a–3d show TREx mosaics with ELFIN's instantaneous locations at four times. During its five-minute pass, ELFIN observed three distinct particle populations: PS, IB, RB, whose approximate locations we annotated above Figure 3e. These three populations can be distinguished using the omnidirectional j as well as the $j_\parallel/j_\perp$ ratio in Figures 3e–3g. Figure 3e shows the spin-resolved 63 keV fluxes, which we binned according to the Text S1 methodology, and show the result in Figures 3f and 3g.

Between 04:17:30-04:20:10 UT ($65° < \lambda < 75°$) Figures 3f and 3g shows isotropic <200 keV electrons which are consistent with the PS region with a small $B_z \leq 5$ nT that ensures electron scattering via FLCS. Similarly, at ~04:20:12, Figure 3f shows a sharp transition between two electron populations with maximum energies rising from 200 keV to >2 MeV. This intense isotropic (presumably FLCS-type) precipitation continues until 04:20:25 UT ($64° < \lambda < 65°$). At this time precipitating flux and flux ratio $j_\parallel/j_\perp$ dropped down during one spin at energies above ~250 keV, indicating the steep IB in this energy range. This may occur due to crossing of large equatorial gradient of magnetic field, that one can visualize as the outer boundary of the dipolarization region (A. V. Artemyev et al., 2024). This is not an unusual observation. Indeed, A. V. Artemyev et al. (2024) showed that 45% of IBs observed by ELFIN had such steep IB in this limited energy range. Earthward of this boundary, the relativistic electrons remained anisotropic (except for a short spike of isotropic fluxes at ~04:20:45 UT), consistent with the enhanced equatorial B_z in the dipolarized region inside of the auroral bulge.

Throughout the entire auroral bulge, until ~04:21:20 ($60° < \lambda < 64°$) the sub-relativistic electrons have high fluxes and isotropic precipitation, likely a whistler-mode driven precipitation (but definitely not FLCS, as proved by empty loss-cone of relativistic electrons). While the relativistic electron loss-cone was empty, ELFIN detected the presence of quasi-trapped <2 MeV electrons. These electrons have energies atypical for the PS (<200 keV) and were not solar energetic particles (Wilson et al., 2024). They are, however, characteristic for the outer RB (Ripoll et al., 2020). The energy-dependent $j_\parallel/j_\perp$ in the poleward section of the RB—with $j_\parallel/j_\perp \sim 1$ at the sub-relativistic energies and $j_\parallel/j_\perp < 1$ at relativistic energies—is a signature of a scattering mechanism that becomes less efficient with increasing energy (Lee et al., 2012; Tsai et al., 2023; Zhang, Angelopoulos, et al., 2022). This is in contrast to the equatorward region of the outer RB, observed after 04:21:24, which had j up to relativistic energies but a low $j_\parallel/j_\perp$ across all energies, indicative of a trapped RB population.

The four TREx mosaics in Figures 3a–3d, together with the ELFIN data in Figures 3f and 3g, relate the locations of the aurora and relativistic electron precipitation. Figure 3a shows that TREx did not observe the bright aurora in the $\delta\lambda = 10°$ latitude range where ELFIN observed the PS. Further equatorward, Figure 3b shows a wavy arc that overlapped with the IB. Then in the time range between Figures 3b and 3c, TREx observed SDA as ELFIN observed the RB precipitation overhead. Lastly, Figure 3d shows the most equatorward snapshot in which TREx did not observe bright aurora, and ELFIN only observed trapped electrons. Combined, this data clearly shows that the bright auroral bulge overlapped with the IB and RB precipitation. ELFIN observed the IB and RB electron spectrum with energies spanning from the instrument's 50 keV lower-limit, up to 2 MeV (which, considering ELFIN's sensitivity, is a lower bound of the upper-limit). This overlap is further supported by a Polar Orbiting Environmental Satellites (POES) pass above TREx a few minutes later, which we show in Figure S3 in Supporting Information S1 and Movie S3.

4. Discussion and Conclusions

In the magnetosphere between 4:17 and 4:20 UT, THEMIS-A was in the pre-midnight sector at $R = 7$ R_E as it observed a dipolarization, injected energetic electrons, electromagnetic waves, and ion flows. Since the ion flow directions alternated between Earthward and anti-Earthward, THEMIS-A was likely in the braking region in the NTR (e.g., Birn et al., 1999; Panov et al., 2010). After 4:20 UT, the magnetic field dipolarized and the substorm activity subsided at THEMIS-A. Taken together, THEMIS-A was initially near the NTR which retreated tailward during the dipolarization (Donovan et al., 2008; Lu et al., 1999).

In the ionosphere, TREx ASIs initially observed a faint pre-breakup arc, which suddenly brightened and then expanded poleward beginning at 4:17 UT, when THEMIS-A observed the dipolarization. The auroral bulge consisted of a dynamic arc at the poleward edge and SDA equatorward of it. During the auroral expansion phase, ELFIN-A passed through the TREx field of view between 4:19-4:22 UT. The poleward arc overlapped with the electron IB precipitation spanning 50 keV - 2 MeV energies, and the equatorward SDA overlapped with the outer RB precipitation spanning similar energies. While prior results show that pulsating aurora, proton aurora, patchy aurora, and omega bands can be associated with relativistic electrons (Kawamura et al., 2021; Miyoshi et al., 2021; Shumko et al., 2021; Shumko, Gallardo-Lacourt et al., 2022), to our knowledge this is the first report of ≤2 MeV electron precipitation associated with the substorm auroral bulge. The 2-MeV energy limit is about a factor of 10 higher than reported by Sivadas et al. (2019) and a factor of 10 to a hundred higher than reported by Gabrielse et al. (2019), Kellerman et al. (2015), and Spanswick et al. (2007). While the 2 MeV number fluxes are much lower than the auroral number fluxes, the relativistic electron energy flux may be comparable since their

energies are much higher. The relative contributions of auroral and energetic electrons, and their impacts on the ionosphere and atmosphere, will be investigated in a follow-on study.

To map the precipitation to its magnetospheric source region we use the IB as a low-altitude tracer of the NTR. Figure 3g shows an abrupt electron IB with $j_\parallel/j_\perp \sim 1$ spanning 50 keV-2 MeV energies at its high-latitude edge, and a monotonically decreasing $j_\parallel/j_\perp$ at its low-latitude edge, suggesting that wave-particle interactions partially obscured the IB's energy-latitude dependence. In addition to wave-particle interactions, A. V. Artemyev et al. (2024) suggest that sharp IB energy-latitude patterns arise from FLCS with a large equatorial gradient of magnetic field. Furthermore, Figure 3f shows that this IB demarcated the footprints of two starkly different j populations: <200 keV consistent with the PS, versus <2 MeV consistent with the RB. When combined, the $j_\parallel/j_\perp$ ratio and j spectra support the interpretation that the electron IB mapped to the NTR. Specifically, the IB mapped to the region separating the dipolar region where MeV electrons were trapped (at least before the dipolarization), and the stretched region where they were rapidly lost via FLCS.

Since the IB and the poleward arc overlapped, and the IB mapped somewhere in the NTR, it follows that the sources of both the IB and the poleward arc originated from the NTR. Furthermore, since the SDA was equatorward of the poleward arc, the SDA must have mapped Earthward of the NTR. Thus, auroral bulge precipitation originated from the newly-dipolarized field lines that threaded the RB and IB. While the precipitation originated from the same region, we cannot comment on how electrons were accelerated to relativistic energies in the first place. It is likely that the precipitating relativistic electrons were already trapped in the inner magnetosphere, and that the dipolarization generated numerous instabilities—such as lower-band chorus waves—which rapidly scattered the trapped RB electrons (e.g., Thorne et al., 2005).

Our results support the long-standing assumption made by Barcus (1965) and Lazutin and Rosenberg (1986) that during a substorm expansion phase, the same magnetic field lines thread both the auroral bulge and the outer RB precipitation regions. Furthermore, although the presented substorm occurred during a geomagnetic storm, Sergeev et al. (2019) used particle data to reach a similar conclusion for a non-storm time substorm, providing evidence that the flux tubes within the auroral bulge are dipolarized enough trap 100 s keV electrons, evident via the partially filled loss-cone. We support these results for the first time using direct measurements of relativistic electrons and the aurora. The $1 - 10$s keV electrons contributed to the auroral light emission, while the relativistic electrons produced X-rays which were absorbed before they reached the ground (e.g., Berland et al., 2023; Woodger et al., 2015). Furthermore, since our result occurred during the substorm expansion phase, it complements (Sivadas et al., 2019) who found that a growth-phase arc marks the outer edge of the outer RB during the substorm growth phase.

We summarize our results with an illustration in Figure 4. Right before the dipolarization, the magnetic field lines were highly stretched and the NTR was near $R = 7 R_E$. The NTR was also near the origin of the faint pre-breakup arc (Sergeev, Nishimura, et al., 2012). Right after the dipolarization the region near $R = 7 R_E$ became highly dipolar and the NTR retreated tailward, trapping a part of the original PS in the dipolarized region (Donovan, 2016; Zou et al., 2024). Thus, during the expansion phase, the source(s) of the poleward arc and IB precipitation were near the NTR, and source(s) of the SDA and RB precipitation were Earthward of the NTR.

In summary, a well-timed triple conjunction during a storm-time substorm expansion phase revealed three insights:

1. During a storm-time substorm, 2 MeV electron precipitation was associated with the auroral bulge,
2. The magnetospheric source region of the auroral bulge and the RB overlapped during this substorm, and
3. We deduce that the source region of the auroral bulge and RB electrons was in the newly dipolarized magnetosphere.

Two follow-up questions arise from these findings. First, why was the dipolarization limited to the inner PS, sparing the $\Delta\lambda = 10°$ segment tailward of the NTR? This configuration is similar to the hybrid state of the magnetotail during steady convection events investigated by Sergeev et al. (1994, 2018). In this configuration, the near-Earth tail is highly-stretched, while it is modestly-stretched tailward. A thin current sheet can form in the near-Earth tail, which is unstable to reconnection and the subsequent near-Earth dipolarization (Sitnov et al., 2019). This interpretation is supported by Beyene and Angelopoulos (2024) who found two very near-Earth reconnection events a few hours after this substorm.
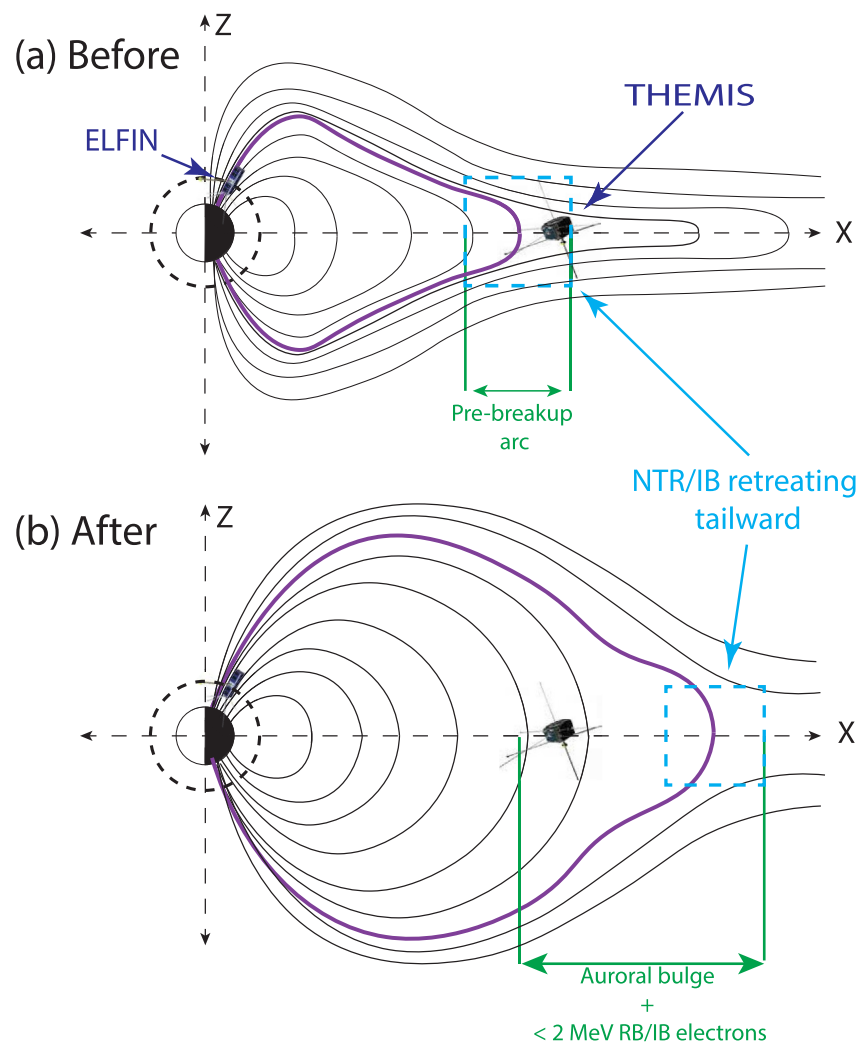
Figure 4. Illustration of the near-Earth magnetic field reconfiguration during this substorm. At $R = 7\ R_E$, THEMIS-A observed the plasma sheet (PS) before (panel a) and after (panel b) the dipolarization. Since the field lines dipolarized at THEMIS-A, this indicates that the NTR, which is represented by the cyan box, retreated tailward. A representative field line connecting the NTR to the ionosphere is colored purple. Before the dipolarization, the NTR mapped to the pre-onset arc. As the NTR retreated, the PS and newly injected electrons inside the dipolarization were accelerated and scattered in the atmosphere, leading to SDA and relativistic radiation belt precipitation observed by TREx and ELFIN-A. The NTR of the dipolarized configuration mapped to the bright poleward arc and the relativistic electron isotropy boundary. Thus, the source of the auroral bulge was at—and Earthward of—the NTR. The illustration is not to scale.

Second, is the overlap between the RB and substorm aurora common? If it is, then during the substorm onset and early expansion phase, the auroral bulge maps to the region where the RB and PS overlap. But we suspect that this is a storm-time effect, and that normally the RB is equatorward of the substorm aurora. The enhanced storm-time ring current likely moved the RB outward, the so-called Dst effect (e.g., D. L. Turner et al., 2012; Ukhorskiy et al., 2015), just enough that it overlapped with the PS. In the overlapping region, multiple acceleration and scattering mechanisms, including wave-mediated Fermi acceleration, could have led to the auroral bulge precipitation (Nakajima et al., 2012). This may be complemented by the tailward shift of the high-energy electron drift shells, which Gabrielse et al. (2019) argued is a result of the changing dB_z/dr during a dipolarization. However, a complicating factor is magnetopause shadowing, which will lead to the loss of the RB electrons on minute time scales (e.g., D. L. Turner & Ukhorskiy, 2020, and references therein). In other words, it remains to be seen if this event is typical and we leave these questions for future work. These questions can be thoroughly addressed with repeated flyovers with satellites equipped with auroral imagers and ELFIN-like particle

instruments, similar to the proposed Cross-Scale INvestigation of Earth's Magnetotail and Aurora (CINEMA) Small Explorer mission concept (Millan & Ukhorskiy, 2024).

Data Availability Statement

The data utilized for this study are publicly available from the following repositories.

1. THEMIS - Angelopoulos (2025b),
2. ELFIN - Angelopoulos (2025a),
3. TREx - Spanswick and Donovan (2023),
4. POES - Rodriguez et al. (2025),
5. SuperMag and OMNI - Gjerloev (2025).

To analyze the satellite data we used the pyspedas library (Grimes et al., 2022) version 1.7.0. To analyze the TREx data we used the asilib library (Shumko, Chaddock et al., 2022) version 0.26.5 which was developed for this study with support from the NASA Heliophysics Tools and Methods Program grant #80NSSC24K0723. Since the Shumko, Chaddock, et al. (2022) publication, asilib includes new features that we summarize in Text S2 in Supporting Information S1. The scripts are organized in a package and archived at Shumko (2025).

References

Akasofu, S.-I. (1964). The development of the auroral substorm. *Planetary and Space Science*, *12*(4), 273–282. https://doi.org/10.1016/0032-0633(64)90151-5

Angelopoulos, V. (2009). *The THEMIS mission*. Springer.

Angelopoulos, V. (2025a). ELFIN data repository [dataset]. *UC Los Angeles*. Retrieved from https://data.elfin.ucla.edu/

Angelopoulos, V. (2025b). THEMIS website [dataset]. *UC Berkley*. Retrieved from https://themis-data.igpp.ucla.edu/

Angelopoulos, V., Cruce, P., Drozdov, A., Grimes, E., Hatzigeorgiu, N., King, D., et al. (2019). The space physics environment data analysis system (spedas). *Space Science Reviews*, *215*, 1–46. https://doi.org/10.1007/s11214-018-0576-4

Angelopoulos, V., Sibeck, D., Carlson, C., McFadden, J., Larson, D., Lin, R., et al. (2008). First results from the themis mission. *Space Science Reviews*, *141*(1–4), 453–476. https://doi.org/10.1007/s11214-008-9378-4

Angelopoulos, V., Tsai, E., Bingley, L., Shaffer, C., Turner, D., Runov, A., et al. (2020). The elfin mission. *Space Science Reviews*, *216*(5), 1–45. https://doi.org/10.1007/s11214-020-00721-7

Angelopoulos, V., Zhang, X.-J., Artemyev, A., Mourenas, D., Tsai, E., Wilkins, C., et al. (2023). Energetic electron precipitation driven by electromagnetic ion cyclotron waves from elfin's low altitude perspective. *Space Science Reviews*, *219*(5), 37. https://doi.org/10.1007/s11214-023-00984-w

Artemyev, A., Angelopoulos, V., Zhang, X.-J., Runov, A., Petrukovich, A., Nakamura, R., et al. (2022). Thinning of the magnetotail current sheet inferred from low-altitude observations of energetic electrons. *Journal of Geophysical Research: Space Physics*, *127*(10), e2022JA030705. https://doi.org/10.1029/2022ja030705

Artemyev, A. V., Demekhov, A., Zhang, X.-J., Angelopoulos, V., Mourenas, D., Fedorenko, Y. V., et al. (2021). Role of ducting in relativistic electron loss by whistler-mode wave scattering. *Journal of Geophysical Research: Space Physics*, *126*(11), e2021JA029851. https://doi.org/10.1029/2021ja029851

Artemyev, A. V., Sergeev, V., Angelopoulos, V., Zhang, X.-J., & Wilkins, C. (2024). Categorization of electron isotropy boundary patterns: Elfin and poes observations. *Journal of Geophysical Research: Space Physics*, *129*(12), e2024JA033231. https://doi.org/10.1029/2024ja033231

Auster, H., Glassmeier, K., Magnes, W., Aydogar, O., Baumjohann, W., Constantinescu, D., et al. (2008). The themis fluxgate magnetometer. *Space Science Reviews*, *141*, 235–264. https://doi.org/10.1007/978-0-387-89820-9_11

Baker, D., Stauning, P., Hones Jr, E., Higbie, P., & Belian, R. (1981). Near-equatorial, high-resolution measurements of electron precipitation at L=6.6. *Journal of Geophysical Research*, *86*(A4), 2295–2313. https://doi.org/10.1029/ja086ia04p02295

Baker, D. N., Pulkkinen, T., Angelopoulos, V., Baumjohann, W., & McPherron, R. (1996). Neutral line model of substorms: Past results and present view. *Journal of Geophysical Research*, *101*(A6), 12975–13010. https://doi.org/10.1029/95ja03753

Barcus, J. (1965). Evidence suggesting dumping of semitrapped electrons on the night side of the Earth. *Journal of Geophysical Research*, *70*(5), 1237–1239. https://doi.org/10.1029/jz070i005p01237

Berland, G., Marshall, R. A., Capannolo, L., McCarthy, M., & Zheng, L. (2023). Kinetic modeling of radiation belt electrons with geant4 to study energetic particle precipitation in earth's atmosphere. *Earth and Space Science*, *10*(11), e2023EA002987. https://doi.org/10.1029/2023ea002987

Beyene, F., & Angelopoulos, V. (2024). Storm-time very-near-earth magnetotail reconnection: A statistical perspective. *Journal of Geophysical Research: Space Physics*, *129*(5), e2024JA032434. https://doi.org/10.1029/2024ja032434

Birn, J., Artemyev, A., Baker, D., Echim, M., Hoshino, M., & Zelenyi, L. (2012). Particle acceleration in the magnetotail and Aurora. *Space Science Reviews*, *173*, 49–102. https://doi.org/10.1007/978-1-4614-6455-6_3

Birn, J., Hesse, M., Haerendel, G., Baumjohann, W., & Shiokawa, K. (1999). Flow braking and the substorm current wedge. *Journal of Geophysical Research*, *104*(A9), 19895–19903. https://doi.org/10.1029/1999ja900173

Birn, J., Nakamura, R., Panov, E., & Hesse, M. (2011). Bursty bulk flows and dipolarization in MHD simulations of magnetotail reconnection. *Journal of Geophysical Research*, *116*(A1), A01210. https://doi.org/10.1029/2010ja016083

Bonnell, J., Mozer, F., Delory, G., Hull, A., Ergun, R., Cully, C., et al. (2009). The electric field instrument (efi) for themis. *The THEMIS mission*, 303–341. https://doi.org/10.1007/978-0-387-89820-9_14

Chen, L., Breneman, A. W., Xia, Z., & Zhang, X.-j. (2020). Modeling of bouncing electron microbursts induced by ducted chorus waves. *Geophysical Research Letters*, *47*(17), e2020GL089400. https://doi.org/10.1029/2020gl089400

Donovan, E. (2016). Coupling between the geomagnetic tail and the inner magnetosphere. In *Space weather fundamentals* (pp. 131–148). CRC Press.

Donovan, E., Liu, W., Liang, J., Spanswick, E., Voronkov, I., Connors, M., et al. (2008). Simultaneous THEMIS in situ and auroral observations of a small substorm. *Geophysical Research Letters*, *35*(17), L17S18. https://doi.org/10.1029/2008gl033794

Dubyagin, S., Sergeev, V., Apatenkov, S., Angelopoulos, V., Runov, A., Nakamura, R., et al. (2011). Can flow bursts penetrate into the inner magnetosphere? *Geophysical Research Letters*, *38*(8), L08102. https://doi.org/10.1029/2011gl047016

Gabrielse, C., Angelopoulos, V., Harris, C., Artemyev, A., Kepko, L., & Runov, A. (2017). Extensive electron transport and energization via multiple, localized dipolarizing flux bundles. *Journal of Geophysical Research: Space Physics*, *122*(5), 5059–5076. https://doi.org/10.1002/2017ja023981

Gabrielse, C., Angelopoulos, V., Runov, A., & Turner, D. L. (2014). Statistical characteristics of particle injections throughout the equatorial magnetotail. *Journal of Geophysical Research: Space Physics*, *119*(4), 2512–2535. https://doi.org/10.1002/2013ja019638

Gabrielse, C., Gkioulidou, M., Merkin, S., Malaspina, D., Turner, D. L., Chen, M. W., et al. (2023). Mesoscale phenomena and their contribution to the global response: A focus on the magnetotail transition region and magnetosphere-ionosphere coupling. *Frontiers in Astronomy and Space Sciences*, *10*, 1151339. https://doi.org/10.3389/fspas.2023.1151339

Gabrielse, C., Harris, C., Angelopoulos, V., Artemyev, A., & Runov, A. (2016). The role of localized inductive electric fields in electron injections around dipolarizing flux bundles. *Journal of Geophysical Research: Space Physics*, *121*(10), 9560–9585. https://doi.org/10.1002/2016ja023061

Gabrielse, C., Kaeppler, S. R., Lu, G., Wang, C.-P., & Yu, Y. (2022). Energetic particle dynamics, precipitation, and conductivity. *Cross-Scale Coupling and Energy Transfer in the Magnetosphere-Ionosphere-Thermosphere System*, 217–300. https://doi.org/10.1016/b978-0-12-821366-7.00002-0

Gabrielse, C., Spanswick, E., Artemyev, A., Nishimura, Y., Runov, A., Lyons, L., et al. (2019). Utilizing the heliophysics/geospace system observatory to understand particle injections: Their scale sizes and propagation directions. *Journal of Geophysical Research: Space Physics*, *124*(7), 5584–5609. https://doi.org/10.1029/2018ja025588

Gillies, D. M., Liang, J., Donovan, E., & Spanswick, E. (2020). The apparent motion of Steve and the picket fence phenomena. *Geophysical Research Letters*, *47*(20), e2020GL088980. https://doi.org/10.1029/2020gl088980

Gjerloev, J. (2012). The superMAG data processing technique. *Journal of Geophysical Research*, *117*(A9), A09213. https://doi.org/10.1029/2012ja017683

Gjerloev, J. (2025). SuperMAG magnetic indices [dataset]. *Johns Hopkins University Applied Physics Laboratory*. Retrieved from https://supermag.jhuapl.edu/indices/

Grimes, E. W., Harter, B., Hatzigeorgiu, N., Drozdov, A., Lewis, J. W., Angelopoulos, V., et al. (2022). The space physics environment data analysis system in python. *Frontiers in Astronomy and Space Sciences*, *9*, 1020815. https://doi.org/10.3389/fspas.2022.1020815

Henderson, M. G. (2009). Observational evidence for an inside-out substorm onset scenario. *Annales Geophysicae*, *27*(5), 2129–2140. https://doi.org/10.5194/angeo-27-2129-2009

Imhof, W., Reagan, J., & Gaines, E. (1979). Studies of the sharply defined l dependent energy threshold for isotropy at the midnight trapping boundary. *Journal of Geophysical Research*, *84*(A11), 6371–6384. https://doi.org/10.1029/ja084ia11p06371

Kamide, Y., & Chian, A. (2007). *Handbook of the solar-terrestrial environment*. Springer.

Kawamura, M., Sakanoi, T., Fukizawa, M., Miyoshi, Y., Hosokawa, K., Tsuchiya, F., et al. (2021). Simultaneous pulsating Aurora and microburst observations with ground-based fast auroral imagers and CubeSat FIREBIRD-II. *Geophysical Research Letters*, *48*(18), e2021GL094494. https://doi.org/10.1029/2021gl094494

Kellerman, A., Shprits, Y., Makarevich, R., Spanswick, E., Donovan, E., & Reeves, G. (2015). Characterization of the energy-dependent response of riometer absorption. *Journal of Geophysical Research: Space Physics*, *120*(1), 615–631. https://doi.org/10.1002/2014ja020027

King, J., & Papitashvili, N. (2005). Solar wind spatial scales in and comparisons of hourly wind and ACE plasma and magnetic field data. *Journal of Geophysical Research*, *110*(A2), A02104. https://doi.org/10.1029/2004ja010649

Lazutin, L. L., & Rosenberg, T. J. (1986). *X-ray emission of auroral electrons and magnetospheric dynamics*. Springer.

Lee, J., Parks, G., Lee, E., Tsurutani, B., Hwang, J., Cho, K., et al. (2012). Anisotropic pitch angle distribution of ~ 100 kev microburst electrons in the loss cone: Measurements from STSAT-1. *Annales Geophysicae*, *30*(11), 1567–1573. https://doi.org/10.5194/angeo-30-1567-2012

Liang, J., Gillies, D., Spanswick, E., & Donovan, E. (2023). Converting TREx-RGB green-channel data to 557.7 nm auroral intensity: Methodology and initial results. *Earth and Planetary Physics*, *8*(1), 258–274. https://doi.org/10.26464/epp2023063

Lopez, R., Sibeck, D., McEntire, R., & Krimigis, S. (1990). The energetic ion substorm injection boundary. *Journal of Geophysical Research*, *95*(A1), 109–117. https://doi.org/10.1029/ja095ia01p00109

Lu, G., Tsyganenko, N., Lui, A., Singer, H., Nagai, T., & Kokubun, S. (1999). Modeling of time-evolving magnetic fields during substorms. *Journal of Geophysical Research*, *104*(A6), 12327–12337. https://doi.org/10.1029/1999ja900145

Lyons, L., & Speiser, T. (1982). Evidence for current sheet acceleration in the geomagnetic tail. *Journal of Geophysical Research*, *87*(A4), 2276–2286. https://doi.org/10.1029/ja087ia04p02276

Lyons, L. R., Zou, Y., Nishimura, Y., Gallardo-Lacourt, B., Angelopoulos, V., & Donovan, E. F. (2018). Stormtime substorm onsets: Occurrence and flow channel triggering. *Earth Planets and Space*, *70*, 1–10. https://doi.org/10.1186/s40623-018-0857-x

McFadden, J., Carlson, C., Larson, D., Ludlam, M., Abiad, R., Elliott, B., et al. (2008). The themis ESA plasma instrument and in-flight calibration. *Space Science Reviews*, *141*(1), 277–302. https://doi.org/10.1007/978-0-387-89820-9_13

McPherron, R. L., Russell, C. T., & Aubry, M. P. (1973). Satellite studies of magnetospheric substorms on August 15, 1968: 9. Phenomenological model for substorms. *Journal of Geophysical Research*, *78*(16), 3131–3149. https://doi.org/10.1029/ja078i016p03131

Millan, R., & Ukhorskiy, S. (2024). Remote-sensing magnetotail dynamics from low Earth orbit with cinema (tech. rep.). *Copernicus Meetings*.

Miyoshi, Y., Hosokawa, K., Kurita, S. e., Oyama, S.-I., Ogawa, Y., Saito, S., et al. (2021). Penetration of MeV electrons into the mesosphere accompanying pulsating aurorae. *Scientific Reports*, *11*(1), 13724. https://doi.org/10.1038/s41598-021-92611-3

Miyoshi, Y., Saito, S., Kurita, S., Asamura, K., Hosokawa, K., Sakanoi, T., et al. (2020). Relativistic electron microbursts as high-energy tail of pulsating Aurora electrons. *Geophysical Research Letters*, *47*(21), e2020GL090360. https://doi.org/10.1029/2020gl090360

Nakajima, A., Shiokawa, K., Sakaguchi, K., Miyoshi, Y., Lee, S., Angelopoulos, V., et al. (2012). Electron and wave characteristics observed by the Themis satellites near the magnetic equator during a pulsating Aurora. *Journal of Geophysical Research*, *117*(A3). https://doi.org/10.1029/2011ja017066

Newell, P. T., Feldstein, Y. I., Galperin, Y. I., & Meng, C.-I. (1996). Morphology of nightside precipitation. *Journal of Geophysical Research*, *101*(A5), 10737–10748. https://doi.org/10.1029/95ja03516

Newell, P. T., & Gjerloev, J. (2011). Evaluation of supermag auroral electrojet indices as indicators of substorms and auroral power. *Journal of Geophysical Research*, *116*(A12), A12211. https://doi.org/10.1029/2011ja016779

Newell, P. T., & Gjerloev, J. W. (2012). SuperMAG-based partial ring current indices. *Journal of Geophysical Research*, *117*(A5), A05215. https://doi.org/10.1029/2012ja017586

Nishimura, Y., Bortnik, J., Li, W., Thorne, R. M., Lyons, L. R., Angelopoulos, V., et al. (2010). Identifying the driver of pulsating Aurora. *Science*, *330*(6000), 81–84. https://doi.org/10.1126/science.1193186

Nishimura, Y., Lessard, M. R., Katoh, Y., Miyoshi, Y., Grono, E., Partamies, N., et al. (2020). Diffuse and pulsating Aurora. *Space Science Reviews*, *216*(1), 1–38. https://doi.org/10.1007/s11214-019-0629-3

Nishimura, Y., Lyons, L., Zou, S., Angelopoulos, V., & Mende, S. (2010). Substorm triggering by new plasma intrusion: Themis all-sky imager observations. *Journal of Geophysical Research*, *115*(A7). https://doi.org/10.1029/2009ja015166

Ohtani, S., Gjerloev, J., McWilliams, K. A., Ruohoniemi, J. M., & Frey, H. U. (2021). Simultaneous development of multiple auroral substorms: Double auroral bulge formation. *Journal of Geophysical Research: Space Physics*, *126*(5), e2020JA028883. https://doi.org/10.1029/2020ja028883

Panov, E., Nakamura, R., Baumjohann, W., Angelopoulos, V., Petrukovich, A., Retinò, A., et al. (2010). Multiple overshoot and rebound of a bursty bulk flow. *Geophysical Research Letters*, *37*(8). https://doi.org/10.1029/2009gl041971

Paschmann, G., Haaland, S., Treumann, R., & Treumann, R. A. (2003). *Auroral plasma physics* (Vol. 15). Springer Science and Business Media.

Raptis, S., Merkin, V., Ohtani, S., Gkioulidou, M., & Regoli, L. H. (2024). Plasma sheet magnetic flux transport during geomagnetic storms. *Geophysical Research Letters*, *51*(18), e2024GL110839. https://doi.org/10.1029/2024gl110839

Reeves, G., Henderson, M., McLachlan, P., Belian, R., Friedel, R., & Korth, A. (1996). Radial propagation of substorm injections. *International conference on substorms*, *389*, 579.

Ripoll, J.-F., Claudepierre, S., Ukhorskiy, A., Colpitts, C., Li, X., Fennell, J., & Crabtree, C. (2020). Particle dynamics in the earth's radiation belts: Review of current research and open questions. *Journal of Geophysical Research: Space Physics*, *125*(5), e2019JA026735. https://doi.org/10.1029/2019ja026735

Rodriguez, J., Redmon, B., & Baugh, K. (2025). NOAA POES and metop space environment monitor (SEM) data [dataset]. *NOAA National Centers for Environmental Information*. Retrieved from https://spdf.gsfc.nasa.gov/pub/data/noaa/noaa18/sem2_fluxes-2sec/

Roux, A., Le Contel, O., Coillot, C., Bouabdellah, A., De La Porte, B., Alison, D., et al. (2008). The search coil magnetometer for Themis. *Space Science Reviews*, *141*(1), 265–275. https://doi.org/10.1007/978-0-387-89820-9_12

Runov, A., Angelopoulos, V., Zhou, X.-Z., Zhang, X.-J., Li, S., Plaschke, F., & Bonnell, J. (2011). A Themis multicase study of dipolarization fronts in the magnetotail plasma sheet. *Journal of Geophysical Research*, *116*(A5). https://doi.org/10.1029/2010ja016316

Samson, J., Lyons, L., Newell, P., Creutzberg, F., & Xu, B. (1992). Proton Aurora and substorm intensifications. *Geophysical Research Letters*, *19*(21), 2167–2170. https://doi.org/10.1029/92gl02184

Sergeev, V., Angelopoulos, V., & Nakamura, R. (2012a). Recent advances in understanding substorm dynamics. *Geophysical Research Letters*, *39*(5), L05101. https://doi.org/10.1029/2012gl050859

Sergeev, V., Apatenkov, S., Nakamura, R., Baumjohann, W., Khotyaintsev, Y. V., Kauristie, K., et al. (2019). Substorm-related near-earth reconnection surge: Combining telescopic and microscopic views. *Geophysical Research Letters*, *46*(12), 6239–6247. https://doi.org/10.1029/2019gl083057

Sergeev, V., Bikkuzina, G., & Newell, P. (1997). Dayside isotropic precipitation of energetic protons. *Annales Geophysicae*, *15*(10), 1233–1245. https://doi.org/10.1007/s00585-997-1233-5

Sergeev, V., Nishimura, Y., Kubyshkina, M., Angelopoulos, V., Nakamura, R., & Singer, H. (2012b). Magnetospheric location of the equatorward prebreakup arc. *Journal of Geophysical Research*, *117*(A1), A01212. https://doi.org/10.1029/2011ja017154

Sergeev, V., Pulkkinen, T. I., Pellinen, R., & Tsyganenko, N. (1994). Hybrid state of the tail magnetic configuration during steady convection events. *Journal of Geophysical Research*, *99*(A12), 23571–23582. https://doi.org/10.1029/94ja01980

Sergeev, V., Sazhina, E., Tsyganenko, N., Lundblad, J., & Søraas, F. (1983). Pitch-angle scattering of energetic protons in the magnetotail current sheet as the dominant source of their isotropic precipitation into the nightside ionosphere. *Planetary and Space Science*, *31*(10), 1147–1155. https://doi.org/10.1016/0032-0633(83)90103-4

Sergeev, V., Tsyganenko, N., Angelopoulos, V., Runov, A., & Singer, H. (2018). Magnetotail configuration during a steady convection event as observed by low-altitude and magnetospheric spacecraft. *Journal of Geophysical Research: Space Physics*, *123*(10), 8390–8406. https://doi.org/10.1029/2018ja025867

Shepherd, S. (2014). Altitude-adjusted corrected geomagnetic coordinates: Definition and functional approximations. *Journal of Geophysical Research: Space Physics*, *119*(9), 7501–7521. https://doi.org/10.1002/2014ja020264

Shevchenko, I., Sergeev, V., Kubyshkina, M., Angelopoulos, V., Glassmeier, K., & Singer, H. (2010). Estimation of magnetosphere-ionosphere mapping accuracy using isotropy boundary and THEMIS observations. *Journal of Geophysical Research*, *115*(A11), A11206. https://doi.org/10.1029/2010ja015354

Shi, X., Stephens, G. K., Artemyev, A. V., Sitnov, M. I., & Angelopoulos, V. (2024). Picturing global substorm dynamics in the magnetotail using low-altitude elfin measurements and data mining-based magnetic field reconstructions. *Space Weather*, *22*(10), e2024SW004062. https://doi.org/10.1029/2024sw004062

Shiokawa, K., Baumjohann, W., & Haerendel, G. (1997). Braking of high-speed flows in the near-earth tail. *Geophysical Research Letters*, *24*(10), 1179–1182. https://doi.org/10.1029/97gl01062

Shumko, M. (2025). Mshumko/elfinasi: First release. https://doi.org/10.5281/zenodo.15678425

Shumko, M., Chaddock, D., Gallardo-Lacourt, B., Donovan, E., Spanswick, E., Halford, A., et al. (2022a). Aurorax, pyaurorax, and aurora-asi-lib: A user-friendly auroral all-sky imager analysis framework. *Frontiers in Astronomy and Space Sciences*, *9*, 1009450. https://doi.org/10.3389/fspas.2022.1009450

Shumko, M., Gallardo-Lacourt, B., Halford, A. J., Blum, L. W., Liang, J., Miyoshi, Y., et al. (2022b). Proton Aurora and relativistic electron microbursts scattered by electromagnetic ion cyclotron waves. *Frontiers in Astronomy and Space Sciences*, *9*, 975123. https://doi.org/10.3389/fspas.2022.975123

Shumko, M., Gallardo-Lacourt, B., Halford, A. J., Liang, J., Blum, L. W., Donovan, E., et al. (2021). A strong correlation between relativistic electron microbursts and patchy Aurora. *Geophysical Research Letters*, *48*(18), e2021GL094696. https://doi.org/10.1029/2021gl094696

Sitnov, M., Birn, J., Ferdousi, B., Gordeev, E., Khotyaintsev, Y., Merkin, V., et al. (2019). Explosive magnetotail activity. *Space Science Reviews*, *215*(4), 1–95. https://doi.org/10.1007/s11214-019-0599-5

Sivadas, N., Semeter, J., Nishimura, Y., & Mrak, S. (2019). Optical signatures of the outer radiation belt boundary. *Geophysical Research Letters*, *46*(15), 8588–8596. https://doi.org/10.1029/2019gl083908

Spanswick, E., & Donovan, E. (2023). Transition region explorer - RGB dataset. *University of Calgary*. https://doi.org/10.11575/4P8E-1K65

Spanswick, E., Donovan, E., Friedel, R., & Korth, A. (2007). Ground based identification of dispersionless electron injections. *Geophysical Research Letters*, *34*(3), L03101. https://doi.org/10.1029/2006gl028329

Spanswick, E., Donovan, E., Liu, W., Wallis, D., Aasnes, A., Hiebert, T., et al. (2005). Substorm associated spikes in high energy particle precipitation. In *The inner magnetosphere: Physics and modeling* (pp. 227–236). American Geophysical Union (AGU). https://doi.org/10.1029/155GM24

Spanswick, E., Reeves, G., Donovan, E., & Friedel, R. (2010). Injection region propagation outside of geosynchronous orbit. *Journal of Geophysical Research*, *115*(A11), A11214. https://doi.org/10.1029/2009ja015066

Thorne, R. M., O'Brien, T., Shprits, Y., Summers, D., & Horne, R. B. (2005). Timescale for MeV electron microburst loss during geomagnetic storms. *Journal of Geophysical Research*, *110*(A9), A09202. https://doi.org/10.1029/2004ja010882

Troyer, R. N., Jaynes, A. N., Kaeppler, S. R., Varney, R. H., Reimer, A. S., & Jones, S. L. (2022). Substorm activity as a driver of energetic pulsating Aurora. *Frontiers in astronomy and space sciences*, *9*, 1032552. https://doi.org/10.3389/fspas.2022.1032552

Tsai, E., Artemyev, A., Angelopoulos, V., & Zhang, X.-J. (2023). Investigating whistler-mode wave intensity along field lines using electron precipitation measurements. *Journal of Geophysical Research (Space Physics)*, *128*(8), e2023JA031578. https://doi.org/10.1029/2023JA031578

Tsai, E., Palla, A., Norris, A., King, J., Russell, C., Ye, S., et al. (2024). Remote sensing of electron precipitation mechanisms enabled by elfin mission operations and adcs. *Advances in Space Research*, *75*(9), 6706–6733. https://doi.org/10.1016/j.asr.2024.07.008

Tsyganenko, N. A. (1989). A magnetospheric magnetic field model with a warped tail current sheet. *Planetary and Space Science*, *37*(1), 5–20. https://doi.org/10.1016/0032-0633(89)90066-4

Turner, D., Claudepierre, S., Fennell, J., O'Brien, T., Blake, J., Lemon, C., et al. (2015). Energetic electron injections deep into the inner magnetosphere associated with substorm activity. *Geophysical Research Letters*, *42*(7), 2079–2087. https://doi.org/10.1002/2015gl063225

Turner, D. L., Shprits, Y., Hartinger, M., & Angelopoulos, V. (2012). Explaining sudden losses of outer radiation belt electrons during geomagnetic storms. *Nature Physics*, *8*(3), 208–212. https://doi.org/10.1038/nphys2185

Turner, D. L., & Ukhorskiy, A. Y. (2020). Outer radiation belt losses by magnetopause incursions and outward radial transport: New insight and outstanding questions from the Van Allen probes era. In *The dynamic loss of earth's radiation belts* (pp. 1–28). Elsevier.

Ukhorskiy, A. Y., Sitnov, M. I., Millan, R. M., Kress, B. T., Fennell, J., Claudepierre, S., & Barnes, R. (2015). Global storm time depletion of the outer electron belt. *Journal of Geophysical Research: Space Physics*, *120*(4), 2543–2556. https://doi.org/10.1002/2014ja020645

Wilkins, C., Angelopoulos, V., Artemyev, A., Runov, A., Zhang, X.-J., Liu, J., & Tsai, E. (2024). Statistical characteristics of the proton isotropy boundary. *arXiv preprint arXiv:2409.04488*.

Wilkins, C., Angelopoulos, V., Runov, A., Artemyev, A., Zhang, X.-J., Liu, J., & Tsai, E. (2023). Statistical characteristics of the electron isotropy boundary. *Journal of Geophysical Research: Space Physics*, *128*(10), e2023JA031774. https://doi.org/10.1029/2023ja031774

Wilson, J., Spence, H., & Schwadron, N. (2024). Solar energetic particles event list. Retrieved from https://hpde.io/NASA/Catalog/LRO/CRaTER/Solar_Energetic_Particles.html

Woodger, L., Halford, A., Millan, R., McCarthy, M., Smith, D., Bowers, G., et al. (2015). A summary of the barrel campaigns: Technique for studying electron precipitation. *Journal of Geophysical Research: Space Physics*, *120*(6), 4922–4935. https://doi.org/10.1002/2014ja020874

Yue, C., Wang, C.-P., Lyons, L., Liang, J., Donovan, E. F., Zaharia, S. G., & Henderson, M. (2014). Current sheet scattering and ion isotropic boundary under 3-d empirical force-balanced magnetic field. *Journal of Geophysical Research: Space Physics*, *119*(10), 8202–8211. https://doi.org/10.1002/2014ja020172

Zhang, X.-J., Angelopoulos, V., Mourenas, D., Artemyev, A., Tsai, E., & Wilkins, C. (2022). Characteristics of electron microburst precipitation based on high-resolution elfin measurements. *Journal of Geophysical Research: Space Physics*, *127*(5), e2022JA030509. https://doi.org/10.1029/2022ja030509

Zhang, X.-J., Artemyev, A., Angelopoulos, V., Tsai, E., Wilkins, C., Kasahara, S., et al. (2022). Superfast precipitation of energetic electrons in the radiation belts of the Earth. *Nature Communications*, *13*(1), 1611. https://doi.org/10.1038/s41467-022-29291-8

Zou, Y., Zhang, X.-J., Artemyev, A. V., Shen, Y., & Angelopoulos, V. (2024). The key role of magnetic curvature scattering in energetic electron precipitation during substorms. *Geophysical Research Letters*, *51*(14), e2024GL109227. https://doi.org/10.1029/2024gl109227